ACS OMEGA

http://pubs.acs.org/journal/acsodf

Review

Electrospun Carbon Nanofibers and Their Applications in Several Areas

Tongtong Wang, Zhe Chen, Weibo Gong, Fei Xu, Xin Song, Xin He,* and Maohong Fan*

Cite This: *ACS Omega* 2023, 8, 22316−22330

Read Online

ACCESS | Metrics & More | Article Recommendations

ABSTRACT: Carbon nanofibers (CNFs) have a broad spectrum of applications, including sensor manufacturing, electrochemical catalysis, and energy storage. Among different manufacturing methods, electrospinning, due to its simplicity and efficiency, has emerged as one of the most powerful commercial large-scale production techniques. Numerous researchers have been attracted to improving the performance of CNFs and exploring new potential applications. This paper first discusses the working theory of manufacturing electrospun CNFs. Next, the current efforts in upgrading the properties of CNFs, such as pore architecture, anisotropy, electrochemistry, and hydrophilicity, are discussed. The corresponding applications due to the superior performances of CNFs are subsequently elaborated. Finally, the future development of CNFs is discussed.

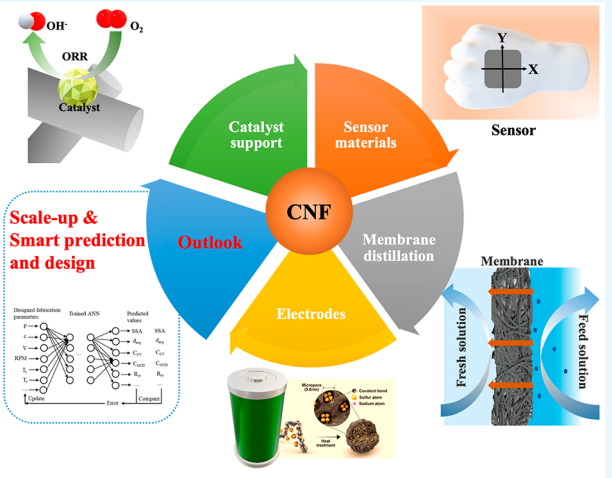

1. INTRODUCTION

Carbon fibers (CFs) are defined by the International Union of Pure and Applied Chemistry (IUPAC) as filaments, lines, or reels that contain more than 92% carbon with a turbostratic nature.[1] Carbon nanofibers (CNFs) are CFs whose sizes are on the magnitude of nanometers. CNFs are high-performance nanostructured carbon materials. They possess not only the inherent properties of carbon nanomaterials (e.g., light weight, excellent mechanical properties, high electrical conductivity, thermal stability, and large specific surface area with compact structure) but also facile processability and controllable preparation and functionalization.[2] They are promising materials with a wide range of applications such as energy, catalysis, and the environment. Therefore, studies on CNFs have been growing for the past ten years. As shown in Figure 1a, the number of publications related to CNFs has increased from 380 in 2012 to 1189 in 2022. There are numerous options for producing CNFs, such as chemical vapor deposition (CVD), templated synthesis, melt spinning, and electrospinning.[3] CVD starts from the chemical reaction between vapor species and deposits a solid-state thin film on a substrate. The templated synthesis produces CNFs on nanostructured templates, and melt spinning involves melting the precursor, and the fiber is extruded through a small orifice. Electrospinning is efficient and facile and has emerged as a promising technique for the commercial-scale production of CNFs.[4] Figure 1a also indicates that among the publications related to CNFs, the percentage of electrospinning-related papers was 30.52% in 2012 and has stabilized at approximately 41% from 2018 to 2021; in 2022, this number jumped to 55%. The term "electrospinning" gained popularity at the end of the 20th century due to researchers such as Doshi and Reneker.[5,6] A basic electrospinning setup consists of a pump that controls the feed of the precursor to a capillary, typically a needle, a collector such as a plate or a drum, and a high-voltage generator that creates an electric field between the needle and the collector. An electric field draws a jet of precursors to the collector, and subsequent heat treatment restructures the precursor and eliminates noncarbon elements, forming a graphene or graphene-like structure. Based on the stacking arrangement of graphene layers, CNFs can have different shapes, such as platelet, tubular, and "herringbone" types.[7] Although CNFs have been commercially produced, technical challenges still exist. For instance, CNFs, if utilized alone, possess insufficient active sites, undermining their catalytic

Received: February 19, 2023
Accepted: May 15, 2023
Published: June 14, 2023

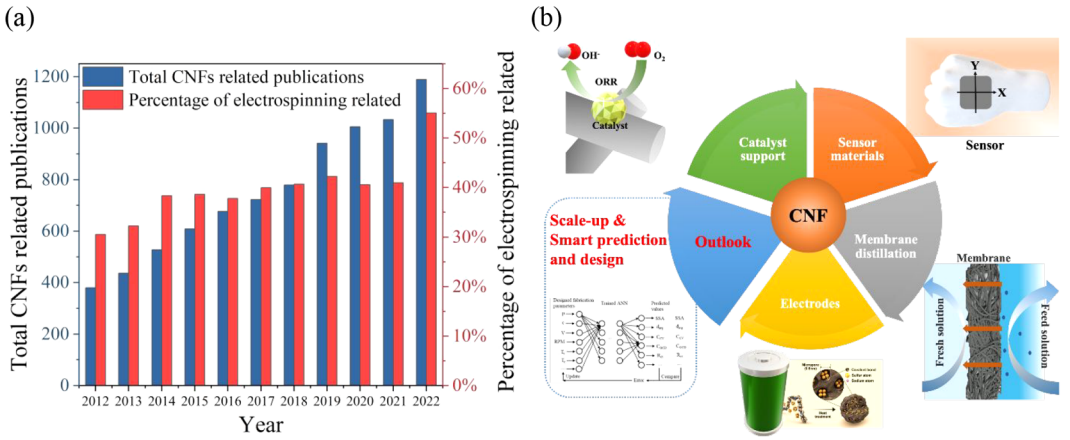

Figure 1. (a) Statistical data of articles related to CNFs published from 2012 to 2022 (data were obtained from Web of Science). (b) Summary of the recent developments of electrospun CNFs discussed in this paper. Copyright 2021 Elsevier.

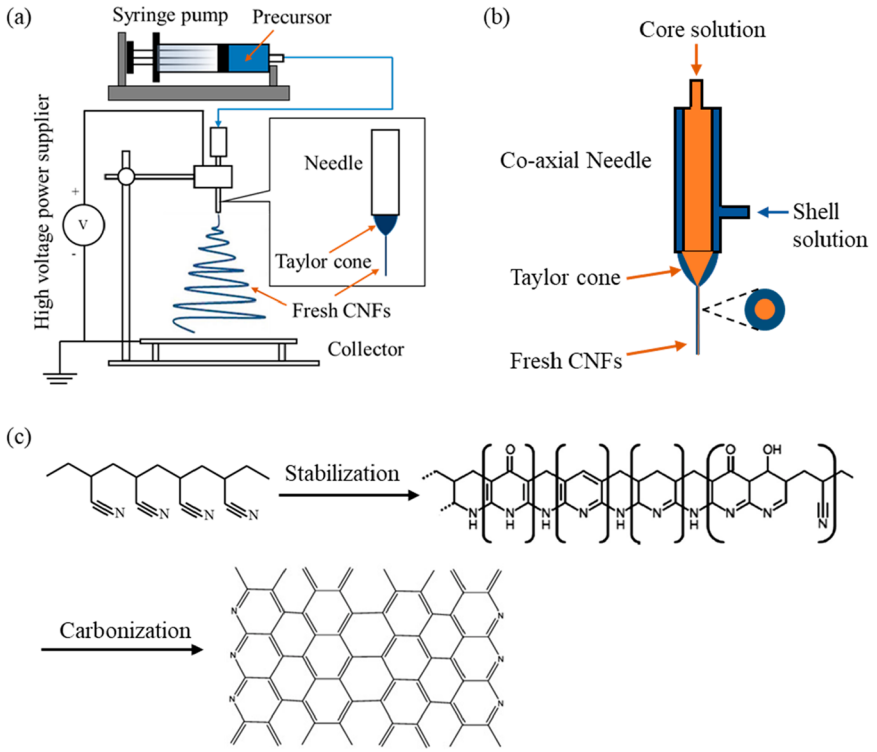

Figure 2. (a) A typical electrospinning setup. (b) A coaxial electrospinning setup.[11,12] (c) Mechanism of heat treatment of fresh CNFs, modified from previous works.[3,13] Copyright 2016, 2022 Elsevier.

effect, randomly electrospun CNFs lack anisotropy and cannot distinguish stimuli (e.g., strains) at different directions, and some CNFs show excellent electrochemical properties but lack flexibility. The development of CNFs includes optimizing their fabrication and exploring their applications. In this paper, we discuss the recent development of the electrospinning process to improve the mechanical properties, catalytic effects, mass transport, and anisotropy of the CNFs. As summarized in Figure 1b, the new applications of CNFs and an outlook on future trends are presented. Incentivized by the higher need for CNFs, more resources will be distributed on scaling up, predicting product properties, and designing fabrication parameters using a combination of an artificial neural network (ANN) and big data is a future trend despite challenges.

2. PROCESS OF ELECTROSPUN CNFS

A typical electrospinning setup is shown in Figure 2a; it comprises a syringe pump, a high-voltage generator, and a collector.[8] The mixture consisting of the substances that form the fibers and chemicals that tune the properties of the fibers is called the precursor. The precursor is dissolved in a solution. During operation, the solution is loaded in the syringe, followed by charging the liquid surface at the needle tip, producing a repulsion against the surface tension. Doing so elongates the originally semispherical surface of the solution and forms a conical shape called a Taylor cone.[9] When the electric field is strong enough to overwhelm the surface tension, a jet is ejected at the tip of the Taylor cone, and before reaching the collector, the solvent evaporates.[6] The fibers

https://doi.org/10.1021/acsomega.3c01114
ACS Omega 2023, 8, 22316−22330

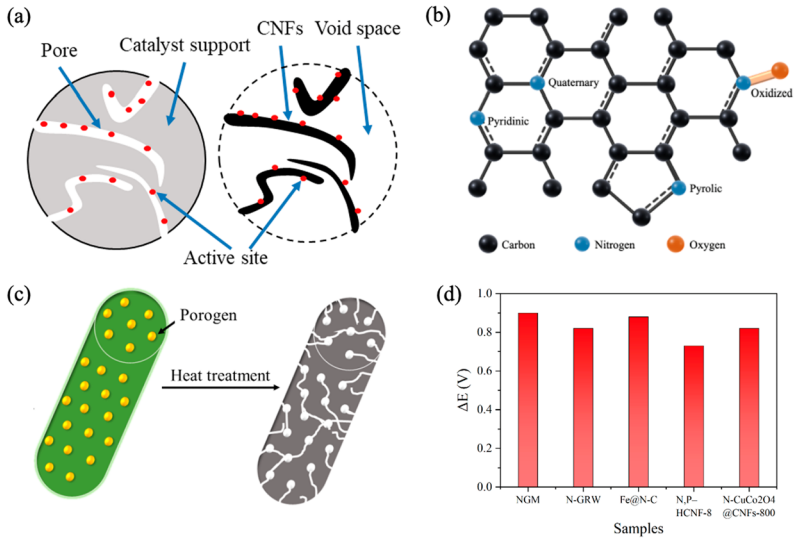

Figure 3. (a) Comparison of the conventional porous and CNFs supports: (left) conventional porous support; (right) CNFs support. Adapted from Chinthaginjala et al.[35] (b) Schematic of N-doped graphene: blue dots, N; red dot, O. (c) Pore-forming mechanism by a heat treating porogen Adapted from Yarova et al.[36] Copyright 2019 MDPI. (d) The charge−discharge voltage gap (ΔV) of other works (NGM, N-GRW, and Fe@N−C), and the works by Gao et al.[30] and Zhang et al.[31] NGM: N-doped graphene mesh, Tang et al.[37] N-GRW: N-doped graphene nanoribbon networks, Yang et al.[27] Fe@N-C: high-density iron nanoparticles encapsulated within a nitrogen-doped carbon nanoshell, Wang et al.[38]

eventually reach and stack on the collector.[12] This collected product is called fresh CNFs; they are heat-treated to create a turbostratic, graphitic structure. The heat treatment includes stabilization, carbonization, and graphitization. The configuration shown in Figure 2a is uniaxial spinning, where the needle only has one precursor solution and no concentric needle. To fabricate hollow CNFs, coaxial, or even multiaxial, spinning is used. Figure 2b shows an example of a coaxial spinning setup; the two needles with different diameters were placed in a coaxial configuration. The larger and smaller needles accept the shell and core solution, respectively. Commonly used precursors include polyacrylonitrile (PAN), polyimide (PI), poly(vinyl alcohol) (PVA), and polyvinyl chloride (PVC);[10] the solutions are usually *N*,*N*-dimethylformamide (DMF), water, etc. This work explains the mechanism of heat treatment using PAN due to its 96% share in carbon fiber market; the schematic is shown in Figure 2c.[10] No matter what precursor is used, the purpose of heat treatment is to form a turbostratic, graphitic structure. Stabilization is done at 180−400 °C under an oxidizing atmosphere. Triple bond C≡N on the side chain of the backbone of PAN breaks into double bond C═N, which creates a ladder-like structure. Carbonization is carried out at 400−1200 °C in an inert atmosphere. This is a pyrolysis process where noncarbon elements are removed, and a graphene-like structure is formed. Coaxial CNFs decompose the core fiber during carbonization, leaving a hollow structure. To improve the graphene-like structure in three dimensions, graphitization is carried out at 1200−2500 °C. However, most studies skip it due to the limitations of the equipment.[8] After heat treatment, fresh CNFs become CNFs. The studies of electrospun CNFs are essentially optimizing the steps mentioned earlier and exploring new applications. For instance, adding metal salts into the precursors can dope active sites onto the surface of CNFs, tuning the carbonization temperature can change the number of heteroatoms that remain on the CNFs, changing the layout of collectors could orderly stack the fibers, increasing anisotropy, and mixing certain ingredients in the precursor can increase the porosity of CNFs due to the thermal decomposition during carbonization.

3. APPLICATION OF CNFs

3.1. Catalyst Support of Hydrogen Fuel Cells and Two-Electron ORR. With the growing need for energy, researchers have been attracted to studying fuel cells. The hydrogen evolution reaction (HER)/oxygen evolution reaction (OER) and the hydrogen oxidation reaction (HOR)/oxygen reduction reaction (ORR) are the main reactions involved in hydrogen fuel cells; a two-electron ORR is also significant in hydrogen peroxide (H_2O_2) production. Although the reaction of oxygen and hydrogen is spontaneous, this process is slow under normal conditions. Therefore, a catalyst is needed to accelerate the reactions.[14] The catalyst frequently used is platinum supported on carbon black (Pt/C).[15] A successful support should have the following features:[16−18] high surface areas to enable high metal dispersion, facile gas accessibility, high electrical conductivity, high stability under cell operation conditions, strong cohesion to catalyst particles, and corrosion resistance. Although carbon black features a high specific surface area and high conductivity, this catalyst suffers from three main disadvantages: oxidation into surface oxide and CO_2,[17] mass transfer limitations,[14] and high cost of Pt. Fortunately, CNFs avoid these obstacles and possess the advantages of carbon black and Pt. Oxidation is a form of corrosion; when it happens, Pt particles will detach and aggregate into larger particles, reducing Pt surface area and undermining cell performance.[14] Jung et al.,[19] Park et al.,[20] and Andersen et al.[21] compared Pt/C and Pt/CNFs as electrodes of polymer electrolyte membrane fuel cells. Cells with Pt/CNFs all exhibited higher stability, indicating that Pt/CNFs had higher corrosion resistance. This was due to the lower hydrophilicity,[22] graphitic structure of each CNF fiber, and the 1D shape of CNFs that did not result in structural collapse when the corrosion was severe. As for the mass transfer issue, CNFs have an open structure, providing more catalyst particle exposure to the reagents. This architecture was suggested by

https://doi.org/10.1021/acsomega.3c01114
ACS Omega 2023, 8, 22316−22330

Schouten et al., as shown in Figure 3a. The CNFs can be considered as an inverse structure of a conventional porous material; since the active sites are located on the open structures, reactants gain easy access. With regard to Pt, extensive research has been conducted to find substitutes, and functionalizing CNFs with other atoms is a promising option. Before electrospinning, dopants can be mixed with precursors (e.g., PAN). The dopants can be heteroatoms such as N, O, and metallic metals and their compounds. Nonmetal heteroatoms (N, B, S, O, P) substitute a small portion of carbon atoms, which alters the charge or spin distribution of the sp^2 carbon plane, and this can facilitate oxygen adsorption or/and subsequent O−O bond breaking.[23] N is considered excellent among the candidates due to its similar atomic size to C and electronic configuration.[24] The schematic of the N-doped graphene structure has been discussed in multiple works[24−26] and can be seen in Figure 3b. The N can be classified into four types: (1) quaternary or graphitic N bonded to three C atoms, (2) pyridinic N bonded to two C atoms at the edge or defect site, (3) pyrrolic N that substitutes C on a pentagonal ring, and (4) oxidized N. Both n- and p-type features coexist on N-doped graphene.[27] An experimental study has pointed out that quaternary N and pyridinic N were responsible for catalyzing the ORR and OER, respectively. Some studies pointed out the N atoms are not active sites, but the C atoms are neighboring quaternary and pyridinic type N. Due to the unpaired electrons released by these N atoms, the neighboring C atoms have the highest spin density and become active sites.[28] As for metals, metal nanoparticles have also been doped on CNFs. Besides heteroatoms, large pore spaces and a large surface are also significant for mass transport, adsorption, and electron transfer. During electrospinning, pore-forming agents (porogens) are often added, and during heat treatment, the porogen vaporizes, leaving large amounts of open holes, as shown in Figure 3c. The large surface area of CNF pore spaces and the rapid electron-transfer capability of graphene[29] make CNFs excellent metal catalyst supports.

By using coaxial electrospinning technology, Gao et al.[30] codoped nitrogen and phosphorus to fabricate hollow CNFs (N,P-HCNFs). This work fabricated metal-free CNF membranes that could serve as an effective electrocatalyst. The core and shell were triphenylphosphine/polyvinylpyrrolidone (TPP/PVP) and dicyandiamide (DCDA)/PAN in this setup, respectively. After heat treatment, a hollow structure in the fiber formed due to the decomposition of the core. The N,P-HCNFs exhibited electrocatalytic activity for the ORR, OER, and HER (i.e., trifunctional), with a low potential deviation, or change−discharge voltage gap (ΔE) of 0.73 V between the half-wave potential ($E_{1/2}$) for the ORR and the potential reaching 10 mA/cm^2 ($E_{j=10}$) for the OER. This was due to the high specific surface area, numerous active sites, and superior mass transfer capability. Zhang et al.[31] reported a method to fabricate N-doped CNFs with a beaded-like structure uniformly decorated with N-doped $CuCo_2O_4$ nanoparticles. The prepared CuCo-MOFs were dissolved with PAN in DMF, followed by electrospinning. The beaded-like structure formed after electrospinning because CuCo-MOFs were encapsulated in 1D fibers. The product was denoted as N-$CuCo_2O_4$@CNFs. N-$CuCo_2O_4$@CNF-800 (carbonized at 800 °C) outperformed commercial RuO_2 and Pt/C for the OER/ORR, in terms of power density (175.6 mW/cm^2), lower discharging−charging voltage gap (0.82 V under 10 mA/cm^2), and long-term cycling stability (120 cycles for 40 h). This beaded-like structure favored electron transportation and mass diffusion, and the homogeneously distributed Cu, Co, and N on the bead increased the exposure of the active sites. As seen in Figure 3d, in the work of Gao et al.[30] and Zhang et al.,[31] the ΔV value matched those of previous non-CNF materials that were metal-free or with metal. Li et al.[32] embedded Ru and Ni within N-doped CNFs (RuNi-NCNFs), which exhibited high electrocatalytic activity for the HER. Due to similar performances and low prices, this material showed promise to replace Pt-based metals. PAN was dissolved in DMF containing $RuCl_3$ and $Ni(NO_3)_2$. After heat treatment, Ru and Ni nanoparticles were homogeneously distributed on the fibers. The assessments of RuNi-NCNFs revealed stability because the polarization curves before and after 4500 cycles of CV tests almost coincided. To achieve 10 mA/cm^2, a cell potential of 1.564 V in overall water splitting was required, outperforming the 1.571 V of Pt/C in the reference group. The excellent performance was due to several reasons: the metallic and ionic Ni and Ru functioned as active sites that promoted the dissociation of water, H−H, and O−H bond generation, heteroatom N (both graphitic N and pyrrolic N) enhanced electron transfer, the porous CNF surface facilitated the electron and mass transport, and the large specific surface area exposed more active sites.

The above examples are four-electron ORRs, and a two-electron ORR is an attractive alternative to the anthraquinone process for H_2O_2 production due to its environmental friendliness. However, like the reactions mentioned above, although noble metals and their alloys are efficient catalysts, high cost prevents their application, and other options suffer from low H_2O_2 selectivity. Li et al.[33] reported a methodology to create carbon nanotubes (NT) encapsulating Ni_3Fe nanoparticles grafted on N-doped nanocarbon fibers (NF), named Ni_3Fe@N-C NT/NFs. PVP, $Ni(NO_3)_2$, and $Fe(NO_3)_3$ were mixed and spun, and the heat treatment carbonized PVP nanofibers into N-doped CNFs and converted metal nitrates into Ni_3Fe nanoparticles. In the HER, the Ni_3Fe@N-C NT/NFs had a low overpotential of 0.72 mV to reach 10 mA/cm^2 in KOH medium and remained stable for 40000 s. A theoretical calculation showed that this material had a favorable Gibbs free energy, −0.14 eV, of hydrogen adsorption, demonstrating high HER activity. The performances arose from abundant active sites, high specific surface area, and excellent mass and electron transfer properties. Dong et al.[34] fabricated honeycomb CNFs (HCNFs) which were superhydrophilic and achieved high activity and selectivity in catalyzing a two-electron ORR. The HCNFs were prepared by electrospinning a mixture of PVA and polytetrafluoroethylene (PTFE). After heat treatment, macropores were created due to the thermal decomposition of PTFE, leaving a honeycomb skeleton. HCNFs showed a water contact angle of 0°. When tested in 0.1 M KOH, it produced H_2O_2 with 97.3% selectivity and an ultrahigh mass activity of 220 A/g at 0.65 V vs RHE (reversible hydrogen electrode), approximately 1.5 times that of the state-of-the-art Co-N_4 incorporated in N-doped graphene (Co_1-NG(O)) catalyst. This results from the rich nanocavities that exposed active sites. The sites have abundant oxygenated edge defects and planar intrinsic carbon defects, and superhydrophilicity, which originated from the oxygenated functional groups and surface topography, conductive carbon network, and high O_2 trapping capability.

Electrospinning enables flexible modification of CNFs, and the porous spaces and low cost made CNFs a competitive candidate for catalyst support in hydrogen fuel cells and the

https://doi.org/10.1021/acsomega.3c01114
ACS Omega 2023, 8, 22316−22330

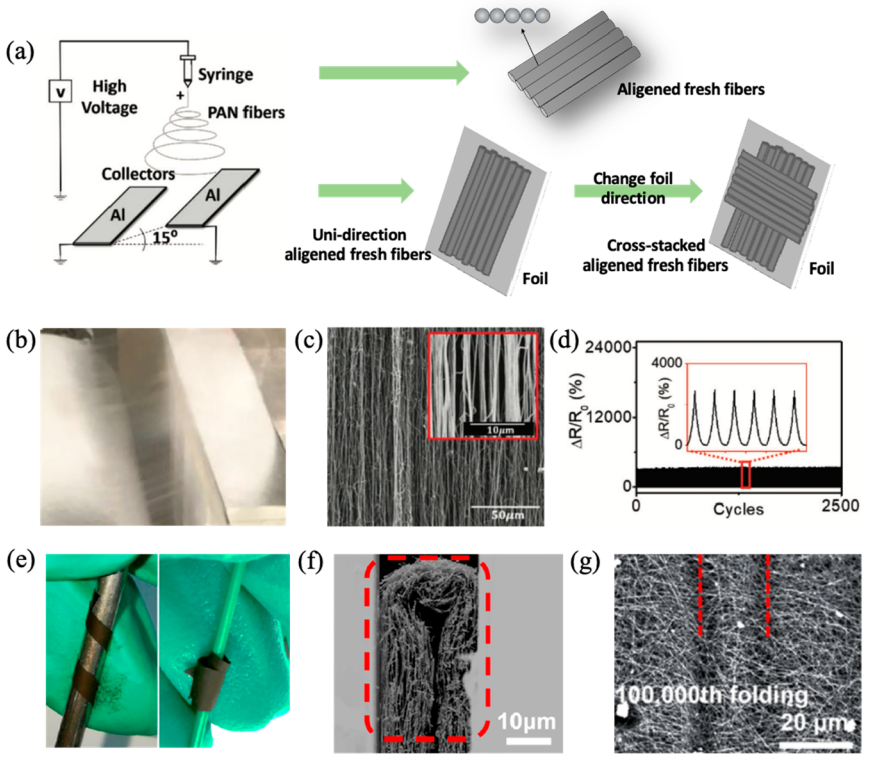

Figure 4. (a) Fabricating orderly stacked CNFs, adapted from Lee et al.[40] Copyright 2019 John Wiley and Sons and Yan et al.[41] (b) Photograph of a suspended, aligned PAN nanofiber film on the inclined gap between two collectors. (c) SEM image of aligned PAN. (d) $\Delta R/R_0$ of the single-layer ACNF strain sensors with CNF alignment parallel to the loading direction for 2500 loading/unloading cycles at 25% strain, showing excellent sensor durability. Adapted from Lee et al.[40] Copyright 2019 John Wiley and Sons. (e) Digital images of crimped and twisted PVA-SFCNFMs. (f, g) SEM images of the folding side of PVA-SFCNFMs and PVA-SFCNFMs after 100000 folding cycles. Adapted from Chai et al.[44] Copyright 2021 American Chemical Society.

two-electron ORR. These features of electrospun CNFs can also be used in other applications such as a Fenton catalyst on water treatment, carbon sequestration, and battery electrodes. The application of CNFs as battery electrodes has been extensively studied due to the growing need for power supply devices and will be discussed later.

3.2. Sensor Material of Wearable Devices. Wearable electronic devices can monitor the human body in real time, providing data such as heart rate, activities during sleep, calories burned, and stress level. These advantages have made wearable devices sought-after products and stimulated numerous types of research. A lightweight, flexible, stretchable, and inexpensive material is very significant for the sensor materials. Conventional semiconductor and metallic materials have the disadvantages of low flexibility, low resolution, and narrow range detection limits.[39] Carbon-based materials such as CNFs and carbon nanotubes (CNTs) have been investigated as highly stable and sensitive sensors due to their excellent conductivity, mechanical properties, etc. Compared to CNTs, CNFs feature cheaper and easier preparation, diverse structures, and facial functionalization. Most importantly, the high surface area of modified CNFs can adsorb more targeted chemicals, resulting in enhanced sensing characteristics.

This paper focuses on anisotropy and flexibility among numerous properties of CNFs as sensor materials of wearable devices. They are the two most representative parameters, and electrospinning enabled their engineering and tuning. Without an intentional change of certain conditions, an electrospinning setup can only produce randomly stacked, isotropic CNFs. These traditional isotropic CNF-based sensors cannot respond differently to stimuli (e.g., strains) from different directions with high sensitivity, which are used to monitor real-time monitoring of personal physiological movements and sophisticated human−machine interfaces. However, orderly stacking CNFs aligns the fibers and results in anisotropy. The electrospinning process enabled orderly stacking by changing the collector configuration or changing the collector RPM. When subject to strains at various directions, the resistance varies due to different deformation or fracturing mechanisms of the CNF. Lee et al.[40] developed a simple and affordable method to produce anisotropic carbon nanofiber (ACNF) films (Figure 4a, upper). Two collectors, one drum and one strip, were used, with one positioned higher than the other, and the two had a 15° inclining gap (Figure 4b,c). Both collectors were connected to the same voltage generator, and thus a split electric field was created. During electrospinning, the higher collector first collected one end of the fibers, and electrostatic force pulled the other end of the fibers to the lower collector. This allowed CNFs to orient across the gap between two collectors.

The subsequent mechanical test of the strain sensor fabricated by ACNFs exhibited a gauge factor (ratio of relative change in electrical resistance R to the mechanical strain ε) of 108, stretchability close to that of human skin, and stable performances over 2500 loading/unloading cycles as shown in Figure 4d. This work also synthesized cross-piled ACNFs by stacking two ACNFs orthogonally, and they possessed a

https://doi.org/10.1021/acsomega.3c01114
ACS Omega 2023, 8, 22316−22330

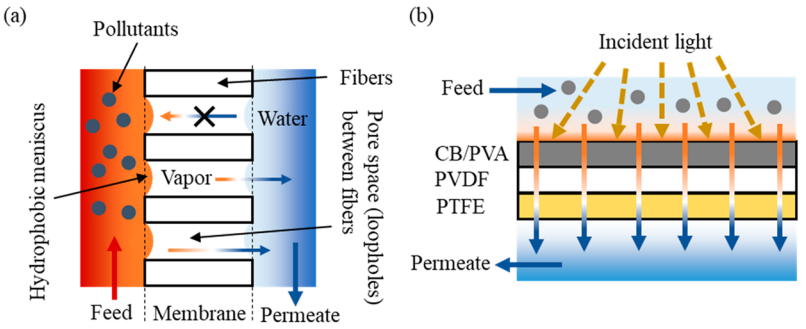

Figure 5. Schematics of (a) general DCMD configuration and (b) solar-driven Janus nanofiber membrane.

selectivity of 3.84 in detecting directions and magnitudes of strains. The performance of the sensor demonstrated a potential for flexible strain sensors for wearable electronics. Yan et al.[41] also synthesized cross-stacked CNFs. PAN was dissolved in DMF with a graphene suspension, making a PAN/graphene precursor. The collection drum's high rotation speed (1000 rpm) achieved the alignment. Zinc foil was wrapped on the drum on which CNFs were stacked; by changing the orientation of the foil, CNFs were cross-stacked (Figure 4a, lower). The fabricated strain sensor could capture a low detection limit (<0.1%) with a gauge factor of 4.24 and a wide strain of up to 130%. The sensor possessed high linearity of up to 40% strain and quick response (<200 ms). This work showed possible broad applications, including body movement monitoring. The anisotropy of CNFs also facilitated directional mass transfer. Sardana et al.[42] fabricated an electrospun anisotropic triboelectric nanogenerator (A-TENG), aligned MXene nanofibers as a negative triboelectric layer, and aligned cellulose acetate NFs (CA NFs) as a positive triboelectric layer. By increasing the rotation speed of the collection drum, the NFs were aligned. The aligned A-TENG had a longer pore length than the randomly aligned triboelectric nanogenerator. This anisotropy enabled fast adsorption/desorption of water molecules and superior antibacterial performance due to the higher drug uptake/release capabilities. This work showed that a anisotropic triboelectric nanogenerator had the potential for a self-powered humidity sensor. Yan et al. prepared an anisotropy of resistance-type strain sensors using an aligned semitransparent graphene-reinforced CNF membrane.[43] The prepared sensor shows a high sensitivity in the parallel direction in the wide strain range of 0.1−38%, with a low sensitivity along the perpendicular direction. An analysis from the microstructures of CNF cracks indicated that the strain levels and sensitivity of the sensor resulted from the aligned degree of CNFs.

Although CNFs exhibit excellent electrical properties, the lack of flexibility prevents them from further applications in the field of sensors. Chai et al.[44] proposed a multistage water management method during heat treatment to make PVA-driven superfoldable CNF membranes (PVA-SFCNFMs). In the process, PVA was mixed with water, creating a PVA hydrocolloid, and was subsequently electrospun. The multistage water management was a heating treatment that hierarchically removed water from the fresh fibers and prevented PVA's melting. This process also prevented the fibers from deformation and cross-linking. The membrane could withstand 180° actual folding for 100000 cycles without structure fracture, and the electrical conductivity remained steady (Figure 4e). PVA-SFCNFMs provided highly sensitive sensing and excellent biocompatible interfaces. Experiments and computer simulations revealed that the mechanism of the superfoldability was due to a "three-level" dispersing stress: on the single-fiber level, aan ppropriate pore structure design was conducive for stress dispersion, between two fiber layers, fibers could slide freely and free voids relieved the bending stress, and between two membranes (each membrane has multiple layers), the bending of a "ω" shape could disperse the stress better than one folding angle (Figure 4f,g). Moreover, anisotropic CNFs lacking foldability could prevent their applications in wearable sensors. Thus, Lee et al. used an electrospun aligned CNF film to assemble a flexible temperature sensor for human health monitoring.[45] The high flexibility of the CNF sensor was due to the low carbonization temperature of 650 °C with an outstanding sensitivity of 1.52% $°C^{-1}$. Also, the greater pyridinic-N content, defects, and disordered sp^2 carbon crystallites in CNFs resulting from the low carbonization temperature enhanced the sensitivity and overcame their low electrical conductivity. In addition, the prepared CNF membrane showed flexible properties but was not strong enough for wearable sensors. Sengupta et al. put a CNF membrane on an optically clear adhesive film layer to fabricate a highly sensitive, flexible, and ultralightweight piezoresistive sensor.[46]

The existing method to prepare the anisotropic CNFs requires specially designed equipment. Thus, the significant challenge in fabricating anisotropic and flexible CNFs is to find a more effective approach to control the direction of a single CNF with a promising scale-up technology. Moreover, the effect of CNFs as wearable devices on human health needs further study.

3.3. Direct Contact Membrane Distillation. Due to the freshwater shortage, researchers have been studying producing freshwater from salt or contaminated water. Conventional technologies such as reverse osmosis consume much energy and have limited application.[47] Membrane distillation (MD) emerged as a competitive option due to facile operation conditions (low temperature and pressure) and excellent performances (high solute rejection, low mechanical requirements). Direct contact membrane distillation (DCMD) has the simplest MD configuration and is widely applied in the desalination process and food industries. In DCMD operation, the membrane has direct contact with the treated water, referred to as the feed, the feed evaporates on the feed side, and the pressure difference across the membrane drives the vapor. The vapor is subsequently removed from the permeate side of the membrane.[48] A temperature gradient also exists across the membrane; the feed side (T_f) temperature is higher than that of the permeate side (T_p). Conventionally, the feed

https://doi.org/10.1021/acsomega.3c01114
ACS Omega 2023, 8, 22316−22330

side or the whole membrane is hydrophobic to prevent the water from penetrating. The membrane acts as a barrier to prevent direct contact between feed and permeate and is also a medium for vapor transfer.[49] A diagram of DCMD is shown in Figure 5a. The membranes of MD should fulfill several requirements. The pore size should be between 10 nm and 1 μm; the porosity should be 70−80%,[50] large enough to increase the permeability and flux but small enough to prevent membrane wetting and formation of a direct liquid bridge across the membrane.[51] The pore space here means the loopholes between the fibers instead of the pores on the fibers. The membranes should also have low thermal conductivity to maintain the temperature difference between feed and permeate.[50,52] Polymeric materials, such as polypropylene (PP), polyvinylidene-fluoride (PVDF), and PTFE, are often used. The conventional production methods include extrusion, rolling and stretching, sintering, and phase separation (i.e., phase inversion).[50] However, these membranes suffer from wetting and fouling caused by contaminants in the feed. For instance, amphiphilic substances can make it facile for feedwater to enter the pores, and surfactants can be adsorbed onto the membranes, converting them to hydrophilic.[49] Fouling is a phenomenon where hydrophobic substances from the feed side enter the pores or deposit on the membrane surface and clog the vapor transfer routes.[53] To prevent fouling, membranes should be modified so that it is difficult for foulants to be adsorbed on the membrane surface. With electrospinning, not only can the precursors be tuned, and multilayer membranes can be spun and each side has contradictory hydrophobicity, referred to as a Janus membrane.[54] Layers could also have different pore sizes and surface roughnesses, which is significant for antifouling. More importantly, the diameters of electrospun nanofibers are submicrometer or nanoscale. The membranes thus have large porosity and dense pores, which is necessary for high flux. PVDF-hexafluoropropylene (PVDF-HFP),[55] PVDF,[56] a PTFE emulsion,[57] PVDF-*co*-hexafluoropropylene (PVDF-PcH)[58] have often been used to synthesize hydrophobic membranes, and CNTs were applied on the membranes to increase hydrophobicity, or PVA was electrospun as a hydrophilic layer.[57] Li et al.[59] proposed a method to fabricate a Janus membrane for DCMD. In this work, the Janus membrane was spun using conventional PAN-based CNFs as a strongly hydrophilic substrate, which was then heat pressed at 140 °C. On one side of this substrate, to apply a hydrophobic layer, a PVDF-*co*-hexafluoropropylene (PH) solution was electrospun, and a polystyrene/poly(dimethylsiloxane) (PS/PDMS) mixed solution was simultaneously electrosprayed to form beads. Tests were conducted at different PS/PDMS ratios, saltwater concentrations, flow rates, and temperatures. In one test, a membrane was prepared with PS/PDMS levels of 7 wt %/7 wt % (concentration in precursor solution), it treated a feed containing 3.5 wt % sodium chloride (NaCl). This feed was heated to 50 °C, and had 0.55 L/min flow rate, the coolant maintained 10 °C and had the same flow rate. This membrane achieved 100% salt rejection, and a maximum 27.7 L/(m^2 h) water flux. When tested with 3.5 wt % NaCl solution with 100 mg/L humic acid as a foulant, the membrane maintained 100% salt rejection efficiency after 36 h of fouling testing. The water flux dropped only by 4%, and the water contact angle dropped only from 148.5 to 135.5°. The competitive water flux and salt rejection efficiency might be attributed to the high porosity (78%) and a compromised thickness (107 μm). The antifouling effect was due to beads, which led to a rough membrane surface and minimized the deposition of foulants. PDMS also endowed the membrane with better antiwetting ability. Without electrospinning, it would be challenging to fabricate such a Janus membrane. Electrospinning produced nanoscale fibers; therefore, the membrane had ideal porosity; this technique also made it facile to control the membrane thickness. In addition, electrospinning allowed simultaneous electrospraying, which stacked HP and PS/PDMS together. Researchers also combined an electrospun DCMD membrane and solar energy. Ju et al.[57] electrospun a solar-driven Janus nanofiber membrane using PTFE as the hydrophobic layer and a mixture of carbon black (CB) and PVA as the hydrophilic layer; the schematic is shown in Figure 5b. A PVDF layer was the intermediate layer between the PTFE and CB-PVA layers to bond them. During experiments, the membrane was irradiated by a solar simulator, the feed passed the CB-PVA layer on the top, and the vapor was produced from the bottom PTFE layer. Contrary to conventional setups, the feed was not heated externally but was heated in situ on the membrane; the CB supplied heat, which converted light to thermal power. The CB-PVA layer functioned as an in situ heater and fouling preventer; the PTFE layer acted as a conventional MD membrane. When irradiated at 1 kW/m^2, the membrane achieved a permeate flux of 1.05 L/(m^2 h), and the salt rejection remained >99.9%; the photoconversion of CB reached 71.4%. Although adding a hydrophilic layer increased the thickness of the membrane and vapor transmission resistance, it reduced heat transfer. The large porosity of PTFE (74 ± 5%) provided large paths for vapor travel. This led to a higher permeate flux than for commercial products (0.4 L/(m^2 h)). When tested with pollutants, including sodium dodecyl sulfate, oil, and $CaCl_2$, for an antifouling performance, the membrane maintained the permeate flux and salt rejection after 60 h. This was because the hydrophobic layer formed strong bonds with water, forming a hydration layer that prevented the adhesion of oil stains. The SEM image also showed that the membrane was easy to clean, and the permeate flux did not drop after cleaning. This indicated that the stacking of fibers avoided the loss of CB particles during cleaning. Fabrication of this membrane was made possible by electrospinning. It stacked nanosized fibers into membranes with high porosities, and stacking also fastened carbon black particles on their positions.

The previous works dealt with fresh polymeric CNFs. A challenge of polymers is corrosion and degradation due to exposure to seawater solar illumination. After heat treatment, some fresh CNFs can become CNFs. CNFs possess a porous structure, light absorption capability, and high corrosion resistance. In addition, electrospinning enables doping, which can alter the hydrophilicity during heat treatment. Yan et al.[60] fabricated a CNF membrane using a PAN and TPA mixture. After heat treatment, N atoms from PAN and O atoms from TPA doped CNFs, making the membrane superhydrophilic. In the MD setup, a nonwoven fabric covered a PS foam floating on feedwater, and the CNF membrane was placed on the fabric. The two ends of the fabric were soaked into the feedwater, which was pumped to the membrane due to a capillary effect. The CNF membrane tested with the help of a solar simulator had a light absorption of 94.2% in the 280−2500 nm wavelength range, a solar energy efficiency (energy transfer to water over the input energy from the simulator) of 89.5%, and a flux of 1.36 kg/(m^2 h) under 1 sun illumination

https://doi.org/10.1021/acsomega.3c01114
ACS Omega 2023, 8, 22316−22330

Table 1. Comparison of Properties of Membranes for DCMD[a]

membrane	fabrication method	q_i	A	C	Q_f	J	t	J_{af}	ref
graphene array-nickel foam, with a polymer coating	plasma-enhanced chemical vapor deposition (PECVD) With commercial polymer, PEDOT-PSS	1	4	3.25	2	1.1	72	1.07 ± 0.09	62
FTCS-CB/PVDF	scalable spraying on commercial PVDF membrane	1	4	natural seawater	3	0.78	48	0.754 ± 0.05	63
PTFE/PP-coated with AF1600 and PDA hydrophilic coating	oxygen plasma treatment, immersion coating, dopamine self-polymerization	Ex[1]	4	simulated seawater	200	19.7	60	16.8	64
PS/PDMS-PH/PAN	electrospinning, hot pressing, and electrospraying	Ex[2]	22.7	3.5	550	27.7	36	27.1	59
CB-PVA/PTFE	electrospinning, hot pressing	1	4	3.5	290	1.05	60	1.035	57
PVDF-HFP-C@CuO/PVDF-HFP	upper layer, electrospun PVDF-HFP membrane consisting of CuO NS decorated with carbon black nanoparticles; bottom layer, PVDF-HFP	1	4.91	3.5		1.88	720	>1.80	61
CNFs	electrospinning, stabilization, and carbonization	1	1	natural seawater		1.36		1.34−1.36	60

[a]Definitions: q_i, incident solar energy intensity, kW/m^2; Ex, external heat; Ex[1], the feed and permeate were maintained at 70 and 20 °C, respectively; Ex[2], the feed and permeate were 50 and 10 °C, respectively; A, effective membrane area, cm^2; C, NaCl concentration, wt %; Q_f, feed flow rate, mL/min; J, permeate flux, kg/(m^2 h); t, time length of antifouling or anticorrosion test, h; J_{af}, permeate flux after antifouling test, kg/(m^2 h); NaCl concentrations of the feed are all 3.5 wt %. Salt rejection rates were all ∼100%. Abbreviations: FTCS, 1*H*,1*H*,2*H*,2*H*-perfluorodecyltrichlorosilane; CB, carbon black; PVDF, polyvinylidene fluoride; PEDOT, poly(3,4-ethylenedioxythiophene); PSS, poly(styrenesulfonate); AF1600, Teflon AF1600, PTFE with amorphous fluoroplastic grade AF1600; PDA, polydopamine.

(1 kW/m^2). It also showed close to 100% purification of ions and organic substances. The performance was due to the dark color of the CNF membrane, superhydrophilicity that enabled facile water transportation, and a pore structure that efficiently retained light and increased the evaporation area. After treatment in acidic, alkaline, and emulsified saline water samples, the flux remained almost the same. That proved the anticorrosion and antifouling of the CNF membrane. The graphene-like structure was chemically stable, and superhydrophilicity helped form a hydration layer. This layer and surface roughness prevented foulant adhesion.[57] Hou et al.[61] proposed a Janus membrane; the bottom layer was hydrophobic, made by electrospinning PVDF-HFP, and the top layer was hydrophilic and light absorbing, made by the same material containing CuO nanosheets decorated with carbon nanoparticles. This membrane was tested by floating on seawater under 1 sun irradiation. It achieved a 1.88 kg/(m^2 h) evaporation rate and remained above 1.80 kg/(m^2 h) without salt precipitation after 30 days of an antifouling test. The excellent performance was because of (1) the synergistic effect of C and CuO, in which the top layer exhibited almost complete absorption at 220−2500 nm light band, (2) the bottom layer formed a stable air cushion and prevented heat transfer loss to bulk water, and (3) the different wettability of two layers only allowed water to transport from the bottom to the top, serving as a unidirectional driving force.

The above works are compared in Table 1. As can be seen, when external heat was used, the permeate flux was higher than when solar light was used in situ. This was because external heat was stable and more powerful. It should also be noted that the feed flow rate did not have an obvious correlation to permeate flux. When solar light was used (i.e., when the input energy density remained unchanged), the permeate flux changed little even after the feed flow rate increased from 2 and 3 to 290 mL/min.

Although electrospun CNFs are promising materials for DCMD, they are hazardous to the human body. The electrospun CNFs contain toxic residue solvents such as DMF, and inhaling CNFs cause lung damage. These concerns need to be solved before commercialization.

3.4. Electrodes. With the high demand for energy and rising concerns about environmental issues, various types of efficient electrochemical energy storage systems have developed rapidly for intermittent power sources (solar, wind, tidal, etc.), especially battery technology. However, both cathode and anode materials face challenges, such as low capacity, decaying performance, and slow charge/discharge. They are caused by tardy and large ions, incompatibilities between electrode and electrolyte, and lack of smooth charge transfer passages.[65−69] Fortunately, CNFs, with their pore architectures, can help solve these issues.

Sodium is a promising substitute for lithium in lithium−sulfur batteries. However, Na−S batteries must work at 300−350 °C to melt sodium and sulfur, which is expensive and dangerous.[70] At room temperature, sodium freezes and slows the reaction; freezing damages the battery due to mechanical stresses.[71] Although a room-temperature sodium−sulfur battery was proposed in 2006,[69] it suffered from low reversible capacity, self-discharging, and serious cycling problems.[72] Moreover, the shuttle effect would cause the loss of redox materials and gradually fade capacity during cycling. This effect refers to the intermediate sodium polysulfides (NaS_x) dissolving into electrolytes.[70,73] The large pore space of CNFs makes them a potential cathode material to host sulfur and accommodate volume changes during cycling, as shown in Figure 6a. Xia et al.[68] proposed carbon hollow nanobubbles on porous carbon nanofibers (CHNBs@PCNFs) as shown in Figure 6b. The precursor was a mixture of PVA and bubbling reagent/porogen lithium nitride (LiN_3). The solution of the precursor was electrospun and heat-treated. Uniform carbon nanobubbles with 2 nm shells derived from the vigorous decomposition of LiN_3 formed on the surface of CNFs with a diameter of ∼200 nm, as shown in Figure 6c. Due to the large pore volume and the carbon matrix that improved the sulfur cathode electrical conductivity, a large amount of sulfur in CHNBs@PCNFs enhanced the energy density of Na-S batteries. The prepared electrode showed a high reversible capacity of 913 mAh/g at 0.1 C, a stable cyclic life of up to 400 cycles, and a remarkable Coulombic efficiency approaching 100%. A density functional theory (DFT) analysis showed a strong interaction between terminal sodium atoms in NaS_x and

https://doi.org/10.1021/acsomega.3c01114
ACS Omega 2023, 8, 22316−22330

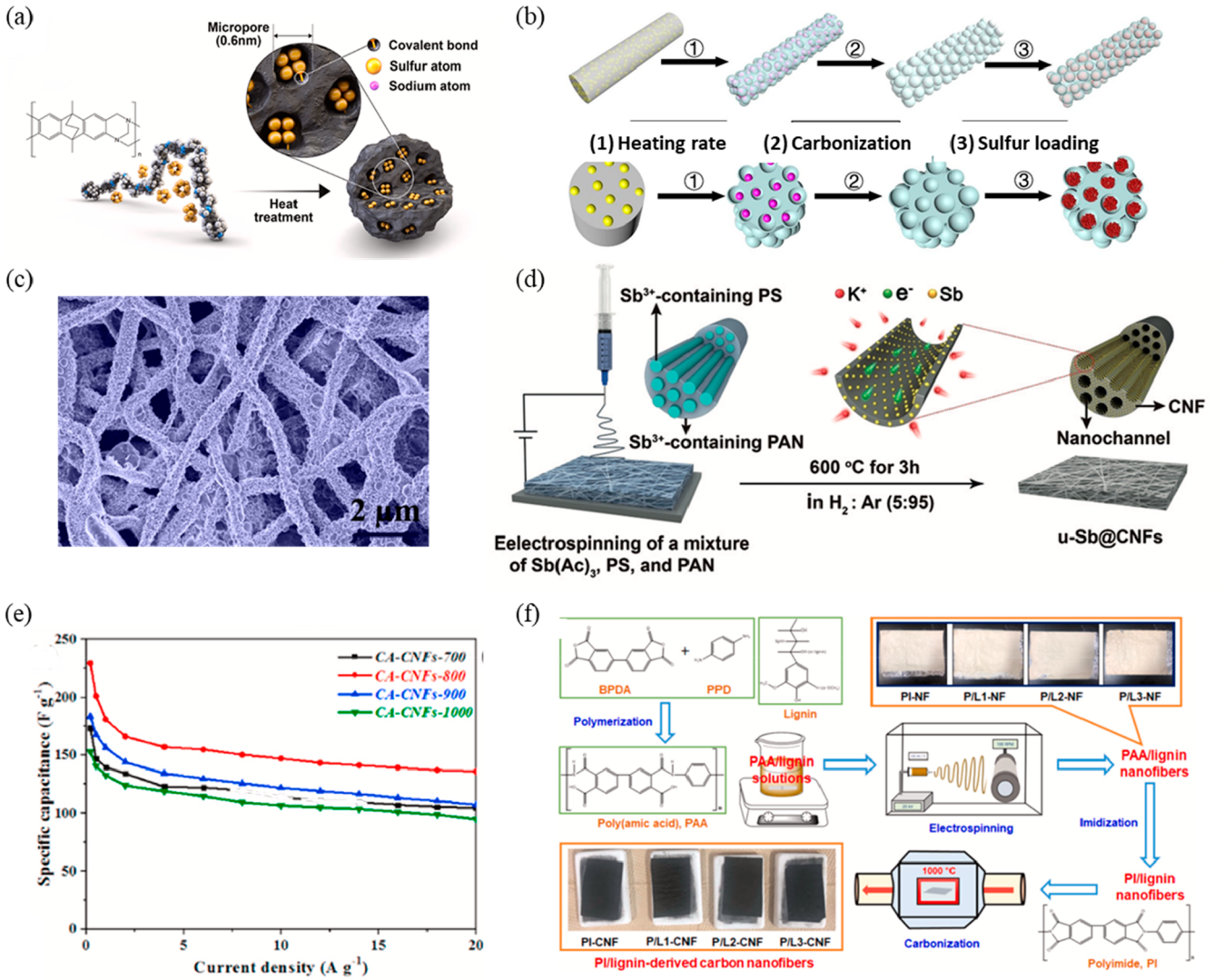

Figure 6. (a) Schematic of PIM-EA-TB-based carbon−sulfur composites preparation procedure. Adapted from Jeon et al.[73] Copyright 2021 Elsevier. (b) Schematic illustration of the preparation of CHNBs@PCNFs and their application as sulfur hosts for room-temperature Na−S batteries. Yellow, pink, and red balls represent LiN_3, Li_3N, and S particles, respectively. Adapted from Xia et al.[68] Copyright 2018 Elsevier. (c) SEM image of PCNFs after calcination of as-electrospun PVA-LiN_3 nanofibers. Adapted from Xia et al.[68] Copyright 2018 Elsevier. (d) Illustration of a simple two-step route to ultrasmall Sb-nanocrystal-impregnated carbon nanofibers containing an array of hollow nanochannels. Adapted from Ge et al.[75] Copyright 2019 John Wiley and Sons. (e) The specific capacitance of CA-CNFs at different current densities. Adapted from Wang et al.[76] Copyright 2022 Elsevier. (f) Schematic procedure for manufacturing CNFs derived from PI/lignin precursors with various ratios of mass via electrospinning and carbonization. Adapted from Park et al.[10] Copyright 2022 Elsevier.

doped N and O atoms; this led to the strong adsorption capability of CHNBs@PCNFs for NaS_x. The adsorption alleviated the shuttle effect. It was further found when they were doped with magnesium hydride (MgH_2), CHNBs@PCNFs could be used as hydrogen storage for a fuel cell with a well-enhanced capacity compared to that when MgH_2 was used alone. The pore structure of CHNBs@PCNFs enabled a homogeneous dispersion of MgH_2 nanoparticles; the open channels also allowed fast hydrogen transportation, and carbon in CHNBs@PCNFs possessed a catalytic effect that facilitated the hydriding and dehydriding performance of MgH_2.

As the candidate anode material of sodium-ion batteries, MoS_2 suffers from slowness during charge/discharge cycles and easy aggregation of the layered structure. To improve the electronic conductivity and solve the agglomeration problem of MoS_2, Liang et al.[66] fabricated nitrogen-doped CNFs (NC) using an electrospinning method and a hydrothermal process to grow MoS_2 nanosheets with sulfur vacancies (MoS_2-VS) on NC. The product was denoted as NC@MoS_2-VS. As an anode material, NC@MoS_2-VS showed a superior capacity of 495 mAh/g for 100 charge/discharge cycles at a current density of 100 mA/g. These performances resulted from the higher sodium ion adsorption energy due to S vacancies and the increase of conductivity of the CNF material. Potassium, like Na, is being extensively studied for potassium-ion batteries. Antimony (Sb) has been considered a promising anode but suffers huge volume variation during charge/discharge cycles, slow potassium ion diffusion, and Sb particle agglomeration.[74] As shown in Figure 6d, Ge et al.[75] encapsulated ultrafine Sb nanocrystals within CNFs (u-Sb@CNFs). The prepared anode showed a notable reversible capacity of 225 mAh/g for 2000 cycles at a current of 1 A/g. The ultrafine Sb nanocrystals and hollow nanochannels enabled fast potassium ion transportation and strain relaxation.

https://doi.org/10.1021/acsomega.3c01114
ACS Omega 2023, 8, 22316−22330

Besides batteries, CNFs have also been extensively used as electrodes for supercapacitors. Compared with other carbon nanomaterials, electrospun CNFs have the unique property of flexible and freestanding supercapacitor electrodes. The performances of these electrodes can be improved by (1) increasing the electrochemical double-layer capacitance by creating a higher specific surface area with a suitable pore size distribution, (2) high electrical conductivity, and (3) endowing pseudocapacitance by introducing defects or heteroatoms and surface modification.[75] As shown in Figure 6e, Wang et al.[76] electrospun cellulose acetate (CA) based CNFs. When carbonized at 800 °C, the CNFs denoted as CA-CNFs-800 possessed an overall optimal electrochemical capacity as a supercapacitor electrode. When the current density was 0.2 A/g, CA-CNFs-800 had the highest specific capacitance of 229.4 F/g, compared to other CNFs carbonized at 700, 900, and 1000 °C whose specific capacitances were no higher than 184 F/g. When the current density was 20 A/g, CA-CNFs-800 capacitance retention was 62.7%, and the values of the other samples were less than 60%. Meanwhile, the charge-transfer resistance of CA-CNFs-800 was only 0.25 Ω, but other samples had a resistance of more than 0.3 Ω. The superior performance was attributed to the synergistic effects of a multiscale porous structure that promoted rapid ion diffusion. A higher specific surface area enabled a higher charge transfer rate and higher specific capacity. Park et al.[10] used a PI and lignin mixture as a precursor to fabricate electrospun CNFs. The PI to lignin mass ratios were 10:0, 9:1, 8:2, and 7:3; the CNFs were denoted as PI-, P/L1, P/L2, and P/L3-CNF. The specific capacitance increased with increasing lignin mass ratio. As the lignin mass ratio increased, the specific capacities increased, and the resistance of the electrode material decreased. P/L3-CNF had the highest specific capacitance of 249 F/g at 1 A/g, and that of other samples was lower than 155 F/g (Figure 6f). The electrical conductivity of this sample was 2.8 S/cm due to its facile ion transportation, while those of others were lower than 1.9 S/cm. A higher lignin content brought about a higher oxygen content on the CNFs, which enhanced the interaction between electrolytes and CNFs, favoring specific capacity. A high oxygen elemental composition also led to defects in the graphitic structures of CNFs.

The electrodes from CNFs are promising in practical applications. However, there are still higher requirements to satisfy, including the scale-up based on the lab research, lower stabilization and carbonization cost, a combination of physical advantages like flexibility and high strength, and design and control of hierarchical pore structures with green and sustainable processes. Thus, renewable resources for the CNFs as electrodes may be a more attractive pathway.

3.5. Other Applications. Electrospun CNFs can also be used to make sensors and treat water pollution because of their excellent physical and chemical properties. The samarium vanadate/CNFs were prepared using a hydrothermal method to determine sulfadiazine. Resulting from the abundant active sites on the surface of CNF and the synergistic effect, the prepared sensors showed excellent properties, such as high sensitivity and selectivity, stability, and low detection limit.[77] The higher specific surface area endowed CNFs with a strong adsorption capacity. Therefore, electrospun CNFs could be used to capture specific pollutants in water by simply modifying the CNFs. The electrospun CNF/graphene oxide composite aerogels were synthesized for oil absorption with an ultralow density (2−3 mg/mL) and great compressibility (80%).[78] Also, the cobalt nanoparticles decorated in N-doped CNF were prepared and used as electromagnetic wave absorbers.[79]

4. OUTLOOK

4.1. Scale up. Scaling up is an important step to commercialization. Numerous companies are committed to industrial or pilot scale equipment for electrospun CNFs, such as nanoScience, Elmarco, and Invovenso.[80,81] Although studies have improved the performances of electrospun CNFs, we still need to overcome obstacles to realizing large-scale production. The issues include but are not limited to small throughput, pollution from solutions,[11] low efficiency, and smoothness of production. Here we introduce three techniques to answer the challenges: multineedle, solvent-free, and needle-free. The multineedle approach can increase the production of CNFs but has the weakness of interferences of the electric field between needles. The spatial separation of needles causes uneven deposition of fibers. Ksapabutr et al.[82] developed a multineedle electrospinning device in which three needles were connected to a slider crank. The needles moved parallel to the rotating drum collector during spinning. This avoided uneven deposition zones. A 24-needle device was made to improve the throughput, and the needles were arranged in a zigzag mode at 500 by 200 mm spacing. The first setup also effectively reduced the electric field interferences and uneven deposition, and the second setup enabled the production of a massive 4.7 m^2 nanofiber fabric. Solvent-free electrospinning has attracted growing attention due to the efficient use of solvent and precursors and being environmentally friendly. In conventional solution electrospinning processes, most of the solvents emit into the atmosphere,[11] and some remain on the fibers. This causes hazards since commonly used solvents such as DMF are toxic. Furthermore, only 8−20 wt % polymers in the precursor were electrospun into fibers.[83] Melt electrospinning is the most typical solvent-free electrospinning technique. Chen et al.[84] developed a polymer melt differential electrospinning (PMDES) device and successfully melted electrospun PP and polylactide; the production efficiency was 500−1000 times that of capillary solution electrospinning, and 80 times that of capillary melt spinning. Meanwhile, applying melt electrospinning to PAN is challenging because PAN degrades before melting at approximately 300 °C;[3,85,86] this prevents commercial melt electrospinning. Including water and/or specific copolymers could reduce the melting point,[3] serving as a possible solution. Needle-based spinning suffers from clogging and may require replacements.[4] Needleless electrospinning emerged as an option to overcome the challenge. Mamun et al.[87] successfully prepared magnetic nanofibers (MNFs) using a needle-free electrospinning setup and a low-toxicity solvent, dimethyl sulfoxide. The magnetism originated from adding iron(II,III) oxide (Fe_3O_4) particles to the PAN precursor. The results showed that the fiber sizes were concentrated in the range100−290 nm. By tuning the parameters, fiber sizes can be changed. This method also showed potential for industrial application due to the lower toxicity of dimethyl sulfoxide.

Although the works mentioned above solved some problems, commercialization still faces safety concerns. The applied voltage is higher than 10 kV, and high voltage is dangerous to operators.[82] Inhalation of CNFs may also pose a health hazard. Animal studies found that when animals were exposed to CNTs and CNFs, adverse lung effects, including

https://doi.org/10.1021/acsomega.3c01114
ACS Omega 2023, 8, 22316−22330

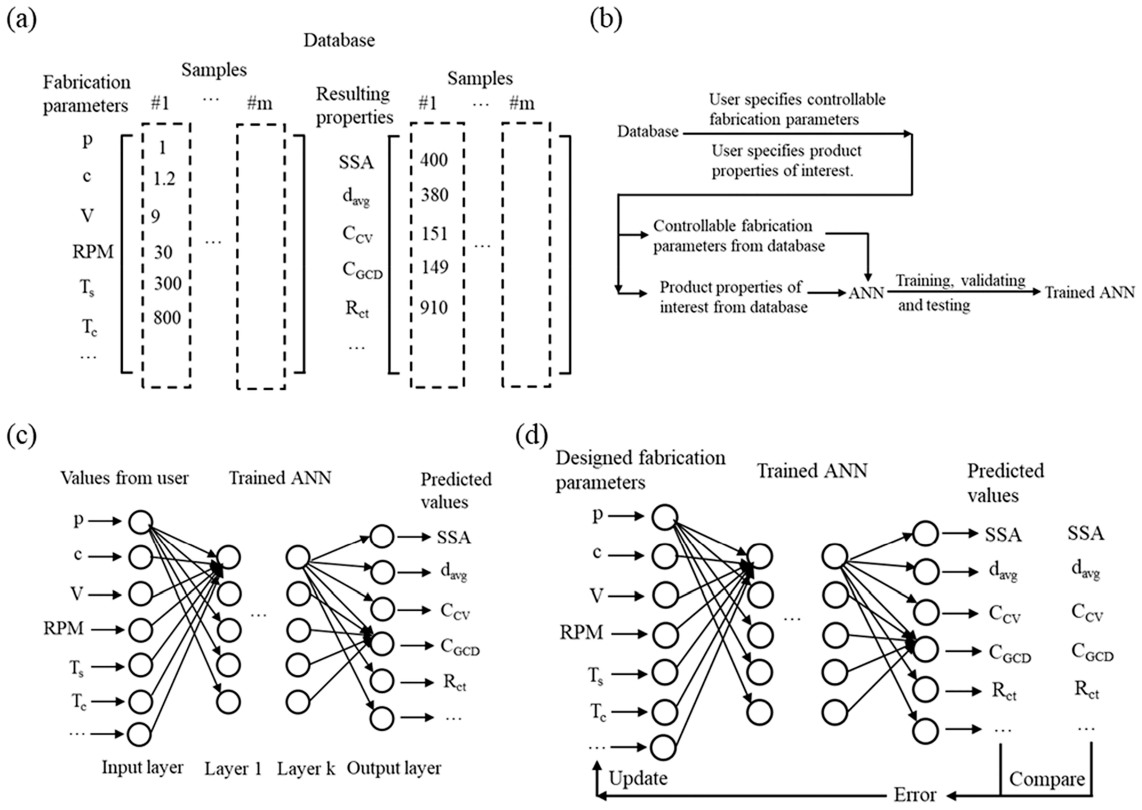

Figure 7. (a) Schematic of a database that contains information on fabrication and resulting properties of CNFs from all sources, where p is the type of precursor and 1 indicates PAN. Commonly used precursors can be encoded. *c* is the concentration of precursor in g/mL. *V* is the voltage in kV. RPM is the rate per minute of collector. 0 indicates a plate collector. T_s is the stabilization temperature in °C. T_c is the carbonization temperature in °C. SSA is the specific surface area in m^2/g. d_{avg} is the average fiber diameter in nm. C_{CV} is the specific capacity calculated from the CV curve in F/g. C_{GCD} is the specific capacity from the GCD curve in F/g. R_{ct} is the specific charge-transfer resistance in Ω/g. *m* is the number of samples. (b) Architecture of the ANN. (c) Workflow of prediction to estimate the properties of CNFs. (d) Designing to calculate the fabrication parameters based on supplied target properties.

inflammation, lung tissue remodeling, and fibrosis, were observed.[88] Mild effects have been observed on human workers handling CNTs/CNFs.[89] Relevant studies are still lacking, and more studies are needed to confirm the correlation between the inhalation of CNTs/CNFs and health conditions.[82] It is also imperative to establish and execute protocols for workers.

4.2. Smart Prediction and Design. All the aforementioned research relied on experiments, and the optimal CNF samples were found by trial and error; this may fit research purposes but is inefficient for industry, which requires different sets of CNF properties based on the goals to be achieved. Finding fabrication parameters and achieving target product properties of CNFs is a daunting task if the conventional trial and error method is utilized. This method consumes time, energy, and budget and produces waste. The inefficiency was due to the complexity of the chemical and physical mechanisms. Establishing a correlation between the fabrication parameters and product properties is challenging. The parameters during fabrications are abundant, including PAN concentration in solution, voltage, needle size, drum RPM, heat treatment temperatures, the ratio of PAN to porogen, etc. The product properties of CNFs can be, for instance, specific capacitance, resistance, or catalytic activity, depending on the interest of the studies. Fortunately, artificial neural networks (ANNs) provide an answer to this problem. Instead of delving into mechanism correlations, finding statistical correlations between fabrication parameters and product properties is less challenging. Here we name our assumption "smart prediction and design". In prediction, a user specifies the fabrication parameters and their values and wants to predict the product properties of interest. The design is the opposite; a user dictates the target product properties and their values and wants to know the value of specified fabrication parameters. A big data database (Figure 7a) contains information on CNFs from publications and manufacturers, including fabrication parameters and product properties. During prediction, the user will first specify the fabrication parameters that need to be controlled and the expected product properties. The data of fabrication parameters and product properties will be sent to the ANN for training, validation, and testing (Figure 7b), which have been extensively discussed by others.[90] The user passes the values of fabrication parameters to the trained ANN to predict product properties (Figure 7c). During design, the ANN will also train, but the user will pass the values of the target product properties to the ANN. The ANN then iterates and returns the designed fabrication parameters and their values, which is an inverse process, as seen in Figure 7d. Some works have been published in predicting CNF product properties. Adabi et al.[91] used an ANN method to identify the effective parameters in predicting cathodic current in a PAN-based CNF electrode. Some CNFs were fabricated by tuning their parameters: layer thickness, electrodeposition time of Pt, etc. Samples were divided into training and testing data,

https://doi.org/10.1021/acsomega.3c01114
ACS Omega 2023, 8, 22316−22330

and ANNs with different architectures were used. The optimal ANN gave a 0.0763 mean square error (MSE) and 0.9563 correlation (R) between the observed and predicted cathodic current using test data. This result proved the validity of an ANN in predicting the performance of CNFs. The CV curve showed that the cathodic current was negatively correlated with CNF diameter, CNF layer thickness, and electrodeposition time of Pt and solution pH. Samadian et al.[92] used an ANN to predict the conductivity of mineralized PAN-based CNFs. After identifying possible influencing fabrication parameters, the ANNs were trained, validated, and tested. The optimal ANN gave an R^2 value of 0.92 during testing.

However, challenges exist for smart prediction and design. The two works mentioned were only predicting, and publications on designing are lacking; designing has more usefulness to research and industry. Furthermore, these works built a database using their experimental data instead of previous results. Arguably the biggest challenge is not the ANN but the database. The data are sporadically distributed inside research papers and industries; mining and organizing the data is complex, and some fabrication parameters are even classified. However, as the CNFs gain more significance, the need for intelligent prediction and design will overwhelm the obstacles.

5. CONCLUSION

The essence of all the development of CNFs is to provide high-performance CNFs that satisfy human needs with the lowest costs in time and money. CNFs have attractive properties such as various pore structures, light weight, and high electrical conductivities. Meanwhile, electrospinning is a flexible and efficient fabrication technique that makes tuning fiber properties possible. Therefore, researchers have been studying new electrospinning techniques, and exploring different applications of electrospun CNFs. Recent progress has been made in the fabrication process of doping heteroatoms, creating anisotropy, changing hydrophilicity, and improving pore spaces and electrical conductivity. They showed superior performances in applications such as catalyst supports, wearable sensing materials, water distillation membranes, and electrodes. Due to the growing need for hydrogen energy, body sensors, fresh water, batteries, etc., continuing to exert the potential of CNFs is always work for the future. However, all the above studies are profitable only when they are commercialized. Commercialization of CNFs relies on scaling up and artificial intelligence plus a database, the former increases the production, and the latter can tremendously accelerate research progress. However, safety, health hazards, and costs are obstacles to scaling up, and data mining is the challenge to smart prediction and designing. In the future, scale-up will focus on "green production", especially solvent-free techniques, cheaper PAN substitutes such as lignin, and application of new energy in heat treatment. The database of CNFs will be established, or the human can circumvent this step and resort to more powerful methods such as generative pretrained transformers (e.g., ChatGPT).

AUTHOR INFORMATION

Corresponding Authors

Xin He − *College of Engineering and Physical Sciences and School of Energy Resources, University of Wyoming, Laramie, Wyoming 82071, United States; College of Materials and Chemistry & Chemical Engineering, Chengdu University of Technology, Chengdu, Sichuan Province 610059, People's Republic of China*; Email: hexin@cdut.edu.cn

Maohong Fan − *College of Engineering and Physical Sciences and School of Energy Resources, University of Wyoming, Laramie, Wyoming 82071, United States; College of Engineering, Georgia Institute of Technology, Atlanta, Georgia 30332, United States*; orcid.org/0000-0003-1334-7292; Email: mfan@uwyo.edu, mfan3@mail.gatech.edu

Authors

Tongtong Wang − *College of Advanced Materials Engineering, Jiaxing Nanhu University, Jiaxing, Zhejiang 314001, People's Republic of China; College of Engineering and Physical Sciences and School of Energy Resources, University of Wyoming, Laramie, Wyoming 82071, United States; Jiaxing key Laboratory of Preparation and Application of Advanced Materials for Energy Conservation and Emission Reduction, Jiaxing Nanhu University, Jiaxing, Zhejiang 314001, People's Republic of China*; orcid.org/0000-0001-5189-951X

Zhe Chen − *College of Engineering and Physical Sciences and School of Energy Resources, University of Wyoming, Laramie, Wyoming 82071, United States*

Weibo Gong − *College of Engineering and Physical Sciences and School of Energy Resources, University of Wyoming, Laramie, Wyoming 82071, United States*

Fei Xu − *College of Advanced Materials Engineering, Jiaxing Nanhu University, Jiaxing, Zhejiang 314001, People's Republic of China; Jiaxing key Laboratory of Preparation and Application of Advanced Materials for Energy Conservation and Emission Reduction, Jiaxing Nanhu University, Jiaxing, Zhejiang 314001, People's Republic of China*

Xin Song − *Faculty of Environmental Science and Engineering, Kunming University of Science and Technology, Kunming 650500, People's Republic of China*; orcid.org/0000-0002-1837-2975

Complete contact information is available at: https://pubs.acs.org/10.1021/acsomega.3c01114

Author Contributions

T.W. and Z.C. contributed equally.

Notes

The authors declare no competing financial interest.

Biographies

Dr. Tongtong Wang received his Ph.D. in Chemical Engineering from the University of Wyoming in 2021. He is now an assistant professor at Jiaxing Nanhu University, Jiaxing, Zhejiang Province. His research interests focus on pitch-derived carbon fibers, carbon nanomaterials, and carbon capture, utilization, and storage.

Zhe Chen received a B.S. degree in 2012 in Oil and Gas Storage and Transportation Engineering from Southwest Petroleum University; he also received an M.S. degree in petroleum engineering from the University of Southern California in 2014. He is currently pursuing a Ph.D. degree in chemical engineering at the University of Wyoming. His research interest is reducing carbon emission by converting carbon materials into value-added products.

Dr. Weibo Gong completed his B.S. and M.S. degrees in 2011 and 2014, respectively, majoring in Chemical Engineering. He received his Ph.D. degree in Chemical Engineering in 2021 from the University of Wyoming. His research interests include (1) catalytic conversion of fossil and renewable resources into value-added chemicals/materials and clean fuels and (2) catalyst design using different methods including supercritical fluids, crystallization, chemical vapor deposi-

https://doi.org/10.1021/acsomega.3c01114
ACS Omega 2023, 8, 22316−22330

tion for synthesis of new functional materials, carbon capture, utilization, and storage (CCUS), and automation process design for chemical reaction system.

Dr. Fei Xu received his bachelor's degree in chemistry at Hunan University in 2011. He completed a Ph.D. in materials physics and chemistry at Fudan University. In 2022, he joined Jiaxing Nanhu University as an assistant professor. His current research interests focus on the design and synthesis of functional polymers and application of organic−inorganic nanocomposite materials for sustainable development.

Dr. Xin Song received a B.S. degree in 2012 majoring in environmental engineering from the Taiyuan Institute of Technology and a Ph.D. degree in environmental engineering from Kunming University of Science and Technology in 2018. He has long-term experience in environmental pollution purification and resource utilization by preparing environmentally friendly catalysts. His recent research is on the preparation and treatment of nano carbon fiber core−shell materials using electrospinning methods. Meanwhile, characterization and quantum chemistry calculation methods are used to study the catalyst characteristics and catalytic reaction mechanisms.

Dr. Xin He received her Ph.D. in Chemical Engineering from the University of Wyoming in 2021. She is now a researcher at Chengdu University of Technology, Chengdu, Sichuan Province. Her research interests focus on carbon materials, CO_2 capture, lithium batteries, phase change materials, and salt lake exploitation.

Dr. Maohong Fan is a Carrell Endowed Chair and SER Professor in Energy and Petroleum, teaches Chemical Engineering at the University of Wyoming, and is an Adjunct Professor at Georgia Tech. As a PI or Co-PI, Dr. Fan has led and co-led many projects in chemical and material synthesis, energy production, and environmental protection areas, including those supported by the U.S. NSF and DOE; among them are carbon capture, utilization, and storage (CCUS), extraction and production of critical materials (including REE & lithium), fossil resource conversion, and renewable energy production and utilization. He has edited and authored more than 350 books, book chapters, special journal issues, and journal papers. He has published in a variety of journals, including *Nature Communications* and *Journal of the American Chemical Society*.

■ ACKNOWLEDGMENTS

This work was supported by the Scientific Research Fund of Zhejiang Provincial Department of Education (Y202250357), Research Funds of Jiaxing Nanhu University (QD61220017 and 62201ZL), the National Natural Science Foundation of China (22006058), the Science & Technology Plan of Sichuan Province (23NSFSC4531), and the University of Wyoming.

■ REFERENCES

(1) Jadhav, S. A.; Dhavale, S. B.; Patil, A. H.; Patil, P. S. Brief overview of electrospun polyacrylonitrile carbon nanofibers: Preparation process with applications and recent trends. *Material Design and Processing Communications* **2019**, *1*, 383.

(2) Liu, R.; Hou, L.; Yue, G.; Li, H.; Zhang, J.; Liu, J.; Miao, B.; Wang, N.; Bai, J.; Cui, Z.; et al. Progress of Fabrication and Applications of Electrospun Hierarchically Porous Nanofibers. *Advanced Fiber Materials 2022 4:4* **2022**, *4*, 604−630.

(3) Newcomb, B. A. Processing, structure, and properties of carbon fibers. *Composites Part A: Applied Science and Manufacturing* **2016**, *91*, 262−282.

(4) Yadav, D.; Amini, F.; Ehrmann, A. Recent advances in carbon nanofibers and their applications - A review. *Eur. Polym. J.* **2020**, *138*, 109963.

(5) Barhoum, A.; Rasouli, R.; Yousefzadeh, M.; Rahier, H.; Bechelany, M. Nanofiber Technology: History and Developments. *Handbook of Nanofibers* **2018**, 1−42.

(6) Doshi, J.; Reneker, D. H. Electrospinning process and applications of electrospun fibers. *J. Electrostat* **1995**, *35*, 151−160.

(7) Rodriguez, N. M.; Chambers, A.; Baker, R. T. K. Catalytic Engineering of Carbon Nanostructures. *Langmuir* **1995**, *11*, 3862−3866.

(8) Nguyen, T. D.; Lee, J. S. Electrospinning-Based Carbon Nanofibers for Energy and Sensor Applications. *Applied Sciences (Switzerland)* **2022**, *12*, 6048.

(9) Taylor, G. Electrically driven jets. *Proceedings of the Royal Society A* **1969**, *313*, 453.

(10) Park, G.-T.; Jeon, H.-B.; Kim, S.-Y.; Gang, H.-E.; Jeong, Y. G. Flexible and self-standing polyimide/lignin-derived carbon nanofibers for high-performance supercapacitor electrode material applications. *Materials Science and Engineering: B* **2022**, *275*, 115530.

(11) *Electrospun Nanofibers*; Springer International: 2022. DOI: 10.1007/978-3-030-99958-2.

(12) Vaseashta, A.; Bölgen, N. *Electrospun nanofibers*; Springer Cham, 2022.

(13) Keshavarz, S.; Okoro, O. V.; Hamidi, M.; Derakhshankhah, H.; Azizi, M.; Mohammad Nabavi, S.; Gholizadeh, S.; Amini, S. M.; Shavandi, A.; Luque, R.; et al. Synthesis, surface modifications, and biomedical applications of carbon nanofibers: Electrospun vs vapor-grown carbon nanofibers. *Coord. Chem. Rev.* **2022**, *472*, 214770.

(14) Zhang, J. *PEM fuel cell electrocatalysts and catalyst layers: Fundamentals and applications*; Springer: 2008. DOI: 10.1007/978-1-84800-936-3.

(15) Wang, Y.; Han, C.; Xie, P.; Li, H.; Yao, P.; Cao, J.; Ruan, M.; Song, P.; Gong, X.; Lu, M.; et al. Highly dispersed PtNi nanoparticles modified carbon black as high-performanced electrocatalyst for oxygen reduction in acidic medium. *J. Electroanal. Chem.* **2022**, *904*, 115908.

(16) Zhou, X.; Qiao, J.; Yang, L.; Zhang, J. A Review of Graphene-Based Nanostructural Materials for Both Catalyst Supports and Metal-Free Catalysts in PEM Fuel Cell Oxygen Reduction Reactions. *Adv. Energy Mater.* **2014**, *4*, 1301523.

(17) Antolini, E. Composite materials: An emerging class of fuel cell catalyst supports. *Appl. Catal., B* **2010**, *100*, 413−426.

(18) Basmadjian, D. *Mass Transfer : Principles and Applications*; CFC Press, 2003.

(19) Jung, J. H.; Park, B. il; Kim, J. Durability test with fuel starvation using a Pt/CNF catalyst in PEMFC. *Nanoscale Res. Lett.* **2012**, *7*, 1−8.

(20) Park, J. H.; Hwang, S. M.; Park, G. G.; Park, S. H.; Park, E. D.; Yim, S. D. Variations in performance-degradation behavior of Pt/CNF and Pt/C MEAs for the same degree of carbon corrosion. *Electrochim. Acta* **2018**, *260*, 674−683.

(21) Andersen, S. M.; Borghei, M.; Lund, P.; Elina, Y. R.; Pasanen, A.; Kauppinen, E.; Ruiz, V.; Kauranen, P.; Skou, E. M. Durability of carbon nanofiber (CNF) & carbon nanotube (CNT) as catalyst support for Proton Exchange Membrane Fuel Cells. *Solid State Ion* **2013**, *231*, 94−101.

(22) Oh, H. S.; Kim, K.; Ko, Y. J.; Kim, H. Effect of chemical oxidation of CNFs on the electrochemical carbon corrosion in polymer electrolyte membrane fuel cells. *Int. J. Hydrogen Energy* **2010**, *35*, 701−708.

(23) Tang, C.; Zhang, Q. Nanocarbon for Oxygen Reduction Electrocatalysis: Dopants, Edges, and Defects. *Adv. Mater.* **2017**, *29*, 1604103.

(24) Kakaei, K.; Esrafili, M. D.; Ehsani, A. *Graphene Surfaces Particles and Catalysts*; Academic Press, 2019.

(25) Wang, D. W.; Su, D. Heterogeneous nanocarbon materials for oxygen reduction reaction. *Energy Environ. Sci.* **2014**, *7*, 576−591.

https://doi.org/10.1021/acsomega.3c01114
ACS Omega 2023, 8, 22316−22330

(26) Li, S.; Yue, G.; Li, H.; Liu, J.; Hou, L.; Wang, N.; Cao, C.; Cui, Z.; Zhao, Y. Pd single atom stabilized on multiscale porous hollow carbon fibers for phenylacetylene semi-hydrogenation reaction. *Chemical Engineering Journal* **2023**, *454*, 140031.
(27) Yang, H. B.; Miao, J.; Hung, S. F.; Chen, J.; Tao, H. B.; Wang, X.; Zhang, L.; Chen, R.; Gao, J.; Chen, H. M. Identification of catalytic sites for oxygen reduction and oxygen evolution in N-doped graphene materials: Development of highly efficient metal-free bifunctional electrocatalyst. *Sci. Adv.* **2016**, *2*, 1.
(28) Ma, R.; Lin, G.; Zhou, Y.; Liu, Q.; Zhang, T.; Shan, G.; Yang, M.; Wang, J. A review of oxygen reduction mechanisms for metal-free carbon-based electrocatalysts. *npj Computational Materials* **2019**, *5*, 1−15.
(29) Bhowmik, K.; Mukherjee, A.; Mishra, M. K.; De, G. Stable ni nanoparticle-reduced graphene oxide composites for the reduction of highly toxic aqueous Cr(VI) at room temperature. *Langmuir* **2014**, *30*, 3209−3216.
(30) Gao, Y.; Xiao, Z.; Kong, D.; Iqbal, R.; Yang, Q. H.; Zhi, L. N,P co-doped hollow carbon nanofiber membranes with superior mass transfer property for trifunctional metal-free electrocatalysis. *Nano Energy* **2019**, *64*, 103879.
(31) Zhang, Y.; Chen, Z.; Tian, J.; Sun, M.; Yuan, D.; Zhang, L. Nitrogen doped CuCo2O4 nanoparticles anchored on beaded-like carbon nanofibers as an efficient bifunctional oxygen catalyst toward zinc-air battery. *J. Colloid Interface Sci.* **2022**, *608*, 1105−1115.
(32) Li, M.; Wang, H.; Zhu, W.; Li, W.; Wang, C.; Lu, X.; et al. RuNi Nanoparticles Embedded in N-Doped Carbon Nanofibers as a Robust Bifunctional Catalyst for Efficient Overall Water Splitting. *Advanced Science* **2020**, *7*, 1901833.
(33) Li, T.; Luo, G.; Liu, K.; Li, X.; Sun, D.; Xu, L.; Li, Y.; Tang, Y. Encapsulation of Ni3Fe Nanoparticles in N-Doped Carbon Nanotube-Grafted Carbon Nanofibers as High-Efficiency Hydrogen Evolution Electrocatalysts. *Adv. Funct Mater.* **2018**, *28*, 1805828.
(34) Dong, K.; Liang, J.; Wang, Y.; Xu, Z.; Liu, Q.; Luo, Y.; Li, T.; Li, L.; Shi, X.; Asiri, A. M.; et al. Honeycomb Carbon Nanofibers: A Superhydrophilic O2-Entrapping Electrocatalyst Enables Ultrahigh Mass Activity for the Two-Electron Oxygen Reduction Reaction. *Angewandte Chemie - International Edition* **2021**, *60*, 10583−10587.
(35) Chinthaginjala, J. K.; Seshan, K.; Lefferts, L. Preparation and application of carbon-nanofiber based microstructured materials as catalyst supports. *Ind. Eng. Chem. Res.* **2007**, *46*, 3968−3978.
(36) Yarova, S.; Jones, D.; Jaouen, F.; Cavaliere, S. Strategies to Hierarchical Porosity in Carbon Nanofiber Webs for Electrochemical Applications. *Surfaces* **2019**, *2*, 159−176.
(37) Tang, C.; Wang, H. F.; Chen, X.; Li, B. Q.; Hou, T. Z.; Zhang, B.; Zhang, Q.; Titirici, M. M.; Wei, F. Topological Defects in Metal-Free Nanocarbon for Oxygen Electrocatalysis. *Adv. Mater.* **2016**, *28*, 6845−6851.
(38) Wang, J.; Wu, H.; Gao, D.; Miao, S.; Wang, G.; Bao, X. High-density iron nanoparticles encapsulated within nitrogen-doped carbon nanoshell as efficient oxygen electrocatalyst for zinc-air battery. *Nano Energy* **2015**, *13*, 387−396.
(39) Sengupta, D.; Romano, J.; Kottapalli, A. G. P. Electrospun bundled carbon nanofibers for skin-inspired tactile sensing, proprioception and gesture tracking applications. *npj Flexible Electronics 2021 5:1* **2021**, *5*, 1−14.
(40) Lee, J. H.; Kim, J.; Liu, D.; Guo, F.; Shen, X.; Zheng, Q.; Jeon, S.; Kim, J. K. Highly Aligned, Anisotropic Carbon Nanofiber Films for Multidirectional Strain Sensors with Exceptional Selectivity. *Adv. Funct Mater.* **2019**, *29*, 1905565.
(41) Yan, T.; Wu, Y.; Tang, J.; Pan, Z. Flexible strain sensors fabricated using aligned carbon nanofiber membranes with cross-stacked structure for extensive applications. *Int. J. Smart Nano Mater.* **2022**, *13*, 432.
(42) Sardana, S.; Singh, Z.; Sharma, A. K.; Kaur, N.; Pati, P. K.; Mahajan, A. Self-powered biocompatible humidity sensor based on an electrospun anisotropic triboelectric nanogenerator for non-invasive diagnostic applications. *Sens Actuators B Chem.* **2022**, *371*, 132507.
(43) Yan, T.; Wu, Y.; Pan, Z. Anisotropy of resistance-type strain sensing networks based on aligned carbon nanofiber membrane. *J. Mater. Sci.* **2021**, *56*, 6292−6305.
(44) Chai, S.; Zan, G.; Dong, K.; Wu, T.; Wu, Q. Approaching Superfoldable Thickness-Limit Carbon Nanofiber Membranes Transformed from Water-Soluble PVA. *Nano Lett.* **2021**, *21*, 8831−8838.
(45) Lee, J. H.; Chen, H.; Kim, E.; Zhang, H.; Wu, K.; Zhang, H.; Shen, X.; Zheng, Q.; Yang, J.; Jeon, S.; et al. Flexible temperature sensors made of aligned electrospun carbon nanofiber films with outstanding sensitivity and selectivity towards temperature. *Mater. Horiz* **2021**, *8*, 1488−1498.
(46) Sengupta, D.; Chen, S. H.; Michael, A.; Kwok, C. Y.; Lim, S.; Pei, Y.; Kottapalli, A. G. P. Single and bundled carbon nanofibers as ultralightweight and flexible piezoresistive sensors. *npj Flexible Electronics* **2020**, *4*, 1−11.
(47) Miao, E. D.; Ye, M. Q.; Guo, C. L.; Liang, L.; Liu, Q.; Rao, Z. H. Enhanced solar steam generation using carbon nanotube membrane distillation device with heat localization. *Appl. Therm Eng.* **2019**, *149*, 1255−1264.
(48) Lawson, K. W.; Lloyd, D. R. Membrane distillation. *J. Membr. Sci.* **1997**, *124*, 1−25.
(49) Huang, Y. X.; Wang, Z.; Jin, J.; Lin, S. Novel Janus Membrane for Membrane Distillation with Simultaneous Fouling and Wetting Resistance. *Environ. Sci. Technol.* **2017**, *51*, 13304−13310.
(50) Khayet, M.; Matsuura, T. *Membrane Distillation: Principles and Applications*; Elsevier: 2011; pp 1−477
(51) Dumée, L. F.; Sears, K.; Schütz, J.; Finn, N.; Huynh, C.; Hawkins, S.; Duke, M.; Gray, S. Characterization and evaluation of carbon nanotube Bucky-Paper membranes for direct contact membrane distillation. *J. Membr. Sci.* **2010**, *351*, 36−43.
(52) Yalcinkaya, F. A review on advanced nanofiber technology for membrane distillation. *J. Eng. Fiber Fabr* **2019**, *14*, 155892501882490.
(53) Liao, Y.; Zheng, G.; Huang, J. J.; Tian, M.; Wang, R. Development of robust and superhydrophobic membranes to mitigate membrane scaling and fouling in membrane distillation. *J. Membr. Sci.* **2020**, *601*, 117962.
(54) Yang, H. C.; Hou, J.; Chen, V.; Xu, Z. K. Janus Membranes: Exploring Duality for Advanced Separation. *Angew. Chem., Int. Ed.* **2016**, *55*, 13398−13407.
(55) Kyoungjin An, A.; Lee, E.-J.; Guo, J.; Jeong, S.; Lee, J.-G.; Ghaffour, N. Enhanced vapor transport in membrane distillation via functionalized carbon nanotubes anchored into electrospun nanofibres. *Scientific Reports* **2017**, *7*, 1−11.
(56) Yan, K. K.; Jiao, L.; Lin, S.; Ji, X.; Lu, Y.; Zhang, L. Superhydrophobic electrospun nanofiber membrane coated by carbon nanotubes network for membrane distillation. *Desalination* **2018**, *437*, 26−33.
(57) Ju, J.; Huang, Y.; Liu, M.; Xie, N.; Shi, J.; Fan, Y.; Zhao, Y.; Kang, W. Construction of electrospinning Janus nanofiber membranes for efficient solar-driven membrane distillation. *Sep Purif Technol.* **2023**, *305*, 122348.
(58) Tijing, L. D.; Woo, Y. C.; Shim, W. G.; He, T.; Choi, J. S.; Kim, S. H.; Shon, H. K. Superhydrophobic nanofiber membrane containing carbon nanotubes for high-performance direct contact membrane distillation. *J. Membr. Sci.* **2016**, *502*, 158−170.
(59) Li, S.; Li, L.; Zhong, J.; Ma, R.; Xu, X.; Wu, H.; Yu, Y. Engineering beads-on-string structural electrospun nanofiber Janus membrane with multi-level roughness for membrane distillation. *Desalination* **2022**, *539*, 115950.
(60) Yan, J.; Xiao, W.; Chen, L.; Wu, Z.; Gao, J.; Xue, H. Superhydrophilic carbon nanofiber membrane with a hierarchically macro/meso porous structure for high performance solar steam generators. *Desalination* **2021**, *516*, 115224.
(61) Hou, L.; Wang, N.; Yu, L. J.; Liu, J.; Zhang, S.; Cui, Z.; Li, S.; Li, H.; Liu, X.; Jiang, L.; et al. High-Performance Janus Solar Evaporator for Water Purification with Broad Spectrum Absorption and Ultralow Heat Loss. *ACS Energy Lett.* **2023**, *8*, 553−564.
(62) Gong, B.; Yang, H.; Wu, S.; Xiong, G.; Yan, J.; Cen, K.; Bo, Z.; Ostrikov, K. Graphene Array-Based Anti-fouling Solar Vapour Gap

https://doi.org/10.1021/acsomega.3c01114
ACS Omega 2023, 8, 22316−22330

Membrane Distillation with High Energy Efficiency. *Nanomicro Lett.* **2019**, *11*, 1−14.
(63) Gong, B.; Yang, H.; Wu, S.; Yan, J.; Cen, K.; Bo, Z.; Ostrikov, K. K. Superstructure-Enabled Anti-Fouling Membrane for Efficient Photothermal Distillation. *ACS Sustain Chem. Eng.* **2019**, *7*, 20151−20158.
(64) Li, M.; Lu, K. J.; Wang, L.; Zhang, X.; Chung, T. S. Janus membranes with asymmetric wettability via a layer-by-layer coating strategy for robust membrane distillation. *J. Membr. Sci.* **2020**, *603*, 118031.
(65) Wang, J.; Luo, C.; Gao, T.; Langrock, A.; Mignerey, A. C.; Wang, C.; et al. An Advanced MoS2/Carbon Anode for High-Performance Sodium-Ion Batteries. *Small* **2015**, *11*, 473−481.
(66) Liang, J.; Wei, Z.; Wang, C.; Ma, J. Vacancy-induced sodium-ion storage in N-doped carbon Nanofiber@MoS2nanosheet arrays. *Electrochim. Acta* **2018**, *285*, 301−308.
(67) Zhao, N.; Wang, C.; Li, B.; Shen, W.; Kang, F.; Huang, Z. H. Construction of flexible lignin/polyacrylonitrile-based carbon nanofibers for dual-carbon sodium-ion capacitors. *J. Mater. Sci.* **2022**, *57*, 11809−11823.
(68) Xia, G.; Zhang, L.; Chen, X.; Huang, Y.; Sun, D.; Fang, F.; Guo, Z.; Yu, X.; et al. Carbon hollow nanobubbles on porous carbon nanofibers: An ideal host for high-performance sodium-sulfur batteries and hydrogen storage. *Energy Storage Mater.* **2018**, *14*, 314−323.
(69) Park, C. W.; Ahn, J. H.; Ryu, H. S.; Kim, K. W.; Ahn, H. J. Room-temperature solid-state sodiumsulfur battery. *Electrochem. Solid-State Lett.* **2006**, *9*, A123.
(70) Kaewmaraya, T.; Hussain, T.; Umer, R.; Hu, Z.; Zhao, X. S. Efficient suppression of the shuttle effect in Na-S batteries with an As2S3 anchoring monolayer. *Phys. Chem. Chem. Phys.* **2020**, *22*, 27300−27307.
(71) Aktaş, A.; Kirçiçek, Y. *Solar Hybrid Systems: Design and Application*; Elsevier: 2021. DOI: 10.1016/B978-0-323-88499-0.00014-8.
(72) Xu, X.; Zhou, D.; Qin, X.; Lin, K.; Kang, F.; Li, B.; Shanmukaraj, D.; Rojo, T.; Armand, M.; Wang, G. A room-temperature sodium-sulfur battery with high capacity and stable cycling performance. *Nature Communications* **2018**, *9*, 1−12.
(73) Jeon, J. W.; Kim, D. M.; Lee, J.; Kim, M. S.; Jeon, M. H.; Malpass-Evans, R.; McKeown, N. B.; Lee, K. T.; Kim, B. G. Shuttle-effect-free sodium-sulfur batteries derived from a Tröger's base polymer of intrinsic microporosity. *J. Power Sources* **2021**, *513*, 230539.
(74) Du, Y.; Zhang, Z.; Xu, Y.; Bao, J.; Zhou, X. Metal Sulfide-Based Potassium-Ion Battery Anodes: Storage Mechanisms and Synthesis Strategies. *Acta Phys. -Chim. Sin* **2022**, *0*, 2205017.
(75) Ge, X.; Liu, S.; Qiao, M.; Du, Y.; Li, Y.; Bao, J.; Zhou, X. Enabling Superior Electrochemical Properties for Highly Efficient Potassium Storage by Impregnating Ultrafine Sb Nanocrystals within Nanochannel-Containing Carbon Nanofibers. *Angew. Chem., Int. Ed.* **2019**, *58*, 14578−14583.
(76) Wang, Y.; Cui, J.; Qu, Q.; Ma, W.; Li, F.; Du, W.; Liu, K.; Zhang, Q.; He, S.; Huang, C. Free-standing porous carbon nanofiber membranes obtained by one-step carbonization and activation for high-performance supercapacitors. *Microporous Mesoporous Mater.* **2022**, *329*, 111545.
(77) Baby, J. N.; Sriram, B.; Wang, S.-F.; George, M. Integration of samarium vanadate/carbon nanofiber through synergy: An electrochemical tool for sulfadiazine analysis. *J. Hazard Mater.* **2021**, *408*, 124940.
(78) Lin, Y.-Z.; Zhong, L.-B.; Dou, S.; Shao, Z.-D.; Liu, Q.; Zheng, Y.-M. Facile synthesis of electrospun carbon nanofiber/graphene oxide composite aerogels for high efficiency oils absorption. *Environ. Int.* **2019**, *128*, 37−45.
(79) Liu, H.; Li, Y.; Yuan, M.; Sun, G.; Li, H.; Ma, S.; Liao, Q.; Zhang, Y. In situ preparation of cobalt nanoparticles decorated in N-doped carbon nanofibers as excellent electromagnetic wave absorbers. *ACS Appl. Mater. Interfaces* **2018**, *10*, 22591−22601.
(80) Omer, S.; Forgách, L.; Zelkó, R.; Sebe, I. Scale-up of electrospinning: Market overview of products and devices for pharmaceutical and biomedical purposes. *Pharmaceutics* **2021**, *13*, 286.
(81) Joshi, B.; Samuel, E.; Kim, Y. il; Yarin, A. L.; Swihart, M. T.; Yoon, S. S. Progress and potential of electrospinning-derived substrate-free and binder-free lithium-ion battery electrodes. *Chemical Engineering Journal* **2022**, *430*, 132876.
(82) Ksapabutr, B.; Panapoy, M. Fundamentals of electrospinning and safety. in *Metal Oxide-Based Nanofibers and Their Applications*; Elsevier: 2022; pp 3−30. DOI: 10.1016/b978-0-12-820629-4.00004-7.
(83) Cao, L.; Su, D.; Su, Z.; Chen, X. Fabrication of multiwalled carbon nanotube/polypropylene conductive fibrous membranes by melt electrospinning. *Ind. Eng. Chem. Res.* **2014**, *53*, 2308−2317.
(84) Chen, M.; Zhang, Y.; Li, H.; Li, X.; Ding, Y.; Bubakir, M. M.; Yang, W. An example of industrialization of melt electrospinning: Polymer melt differential electrospinning. *Advanced Industrial and Engineering Polymer Research* **2019**, *2*, 110−115.
(85) Frushour, B. G. Melting behavior of polyacrylonitrile copolymers. *Polymer Bulletin* **1984**, *11*, 375−382.
(86) Slade, P. E. The melting of polyacrylonitrile. *Thermochim. Acta* **1970**, *1*, 459−463.
(87) Mamun, A.; Klöcker, M.; Blachowicz, T.; Sabantina, L. Investigation of the Morphological Structure of Needle-Free Electrospun Magnetic Nanofiber Mats. *Magnetochemistry 2022, Vol. 8, Page 25* **2022**, *8*, 25.
(88) Centers for Disease Control and Prevention (CDC). Occupational Exposure to Carbon Nanotubes and Nanofibers. *Current Intelligence Bulletin 65* (2013).
(89) Bergamaschi, E.; Garzaro, G.; Jones, G. W.; Buglisi, M.; Caniglia, M.; Godono, A.; Bosio, D.; Fenoglio, I.; Canu, I. G. Occupational Exposure to Carbon Nanotubes and Carbon Nanofibres: More Than a Cobweb. *Nanomaterials* **2021**, *11*, 745.
(90) Zhang, Z. Artificial Neural Network. *Multivariate Time Series Analysis in Climate and Environmental Research* **2018**, 1−35.
(91) Adabi, M.; Saber, R.; Naghibzadeh, M.; Faridbod, F.; Faridi-Majidi, R. Parameters affecting carbon nanofiber electrodes for measurement of cathodic current in electrochemical sensors: an investigation using artificial neural network. *RSC Adv.* **2015**, *5*, 81243−81252.
(92) Samadian, H.; Zakariaee, S. S.; Adabi, M.; Mobasheri, H.; Azami, M.; Faridi-Majidi, R. Effective parameters on conductivity of mineralized carbon nanofibers: an investigation using artificial neural networks. *RSC Adv.* **2016**, *6*, 111908−111918.

https://doi.org/10.1021/acsomega.3c01114
ACS Omega 2023, 8, 22316−22330